

## Employing a Combination of a Double-Glazed Flat Solar Collector and Sensible Heat Storage for Drying Agricultural Products

Mohamad Efendi<sup>1\*</sup>, Yusuf Hendrawan<sup>2\*</sup>, La Choviya Hawa<sup>2</sup>, Bambang Dwi Argo<sup>2</sup>

<sup>1</sup> Agroindustrial Technology Department, Faculty of Agricultural Technology, Universitas Brawijaya, Malang, East Java, Indonesia

<sup>2</sup> Agricultural Engineering and Biosystem Department, Faculty of Agricultural Technology, Universitas Brawijaya, Malang, East Java, Indonesia

\* Corresponding author's e-mail: mohamadefendi231199@gmail.com; yusuf\_h@ub.ac.id

### ABSTRACT

Convection heat collector technology is a promising technology for drying agricultural products. The study aimed to determine the temperature characteristics, energy efficiency, and thermal discharging of a flat plate-type collector using double-glazing technology integrated with heat storage material in the state of iron scraps in passive and active modes. Investigation was conducted for seven hours of exposure under the sun (08:00–15:00 local time). Ten temperature sensors and four humidity sensors were used during measurements to determine the thermal characteristics of the heat collector. The density of iron scraps as heat storage material is 250 kg/m<sup>3</sup> with an irradiation time of seven hours. The results indicate that the passive mode of operation has a higher temperature characteristics than the active mode. During irradiation process, the highest temperatures on the absorber in active and passive modes were 63 °C and 55 °C, respectively. Meanwhile, the highest temperatures on the TES in passive and active modes during irradiation were 55.6 °C and 50.6 °C, respectively. The energy efficiency of the collector ranges from 23.3–55.1% (passive) and 18.6–40.7% (active). The energy efficiency of the TES (Thermal Energy Storage) has a range of 7.4–22.7% (passive) and 7.4–13.0% (active). During discharging process, it shows that the TES in passive mode can store heat for 275 minutes and active mode for 95 minutes. Heat collectors that used double glazing technology and heat storage materials using iron scraps with a density of 250 kg/m<sup>3</sup> have a significant potential to extend the drying duration of agricultural products with limited exposure to sunlight and environmentally friendly heat collectors.

**Keywords:** force convection, iron scraps, natural convection, sensible heat storage, solar collector, thermal energy storage.

### INTRODUCTION

The heat collector technology utilizing solar radiation heat has significant potential for drying agricultural products (Fterich et al., 2018; Mahapatra and Tripathy 2019). Given the abundance of solar energy and its accessibility to all, collector technology emerges as a viable alternative for harnessing solar energy effectively, while mitigating pollution concerns (Chen et al., 2021; Fterich et al., 2018; Krishnananth and Kalidasa 2013), free to use (Bennour and Mzad 2022), energy sustainability (Zhou et al., 2023; Borzuei et al., 2021), and the energy demand continues to

increase every year (Mokhlif et al., 2021). This type of technology has long been utilized and continues to change to improve the work efficiency of the collector itself. Nowadays, various types of convection and conduction-type collectors have been developed. Convection technology is one type of collector that is widely used. This technology was selected due to its ease of manufacture and replication, as well as its straightforward application in the field. Heat collectors can be applied for several needs, such as drying agricultural products, greenhouse heating, room heating, water heating, water desalinization to obtain potable water (Mokhlif et al., 2021; Subiantoro

and Ooi 2013; Yang et al., 2023) and solar cooling (Marc et al., 2011). Drying agricultural products has excellent potential using natural convection heat collectors (Fterich et al., 2018). The designation in drying agricultural products can be directly applied without additional energy (Ammar et al., 2022). In addition, forced convection heat collectors also have the potential to be used because they can speed up the product drying process.

The convection type itself is also divided into forced and natural type collectors. The forced convection type requires mechanical assistance, such as a fan or blower in a large air volume. Environmental air is forced into the collector chamber until a temperature increase and then exits to be used as air circulation in the drying chamber. Natural convection technology has the advantage of being environmentally friendly, having minimal cost, high-temperature achievement, and high efficiency (Ehrmann et al., 2013). Although natural-type heat collectors in solar dryers can be applied, food product drying systems cannot quickly move a large amount of water.

The additional component of moving air quickly with a fan or blower requires a large amount of additional energy and is not environmentally friendly (Prakash and Kamatchi 2023). The amount of fossil energy used contributes to this condition. The use of environmentally-friendly flat plate collectors with natural convection must be implemented and developed. This case has the potential to be a promising alternative solution in the future. Some research results using natural convection collector systems are reports (Ammar et al., 2022), which can provide up to 68% collector efficiency during the day. In addition, the results of research conducted by (Prakash and Kamatchi 2023) provide collector efficiency up to 66.32% and (Panwar 2014) with an efficiency of 37.93%. Research by (Mokhlif et al., 2021) informed that the heat collector with double glazing for water heating has a thermal efficiency of 68% with a mass flow rate of 0.0091 kg/s. In addition, the application of forced convection has been reported by (Hawa et al., 2021; Mardiyani et al., 2019) for drying agricultural products. (Fterich et al., 2018) also reported that the forced convection type solar dryer can provide a thermal efficiency of up to 65% and an electrical efficiency of about 12%.

Thermal energy storage (TES) is essential to thermal energy management. In the situations where solar heat is unavailable, a necessity for thermal energy utilization, facilitated by thermal

insulation and storage materials arises (Yang et al., 2023). The material requirements used are the material that can absorb energy and store the energy in the long term period. This stored energy is then taken slowly according to the needs of the heat storage material until the heat runs out. Thermal energy storage is generally divided into three types, namely thermochemical energy storage, latent heat energy storage, and sensible heat energy storage (Wang and Xie 2022). Although thermochemical and latent heat storage have superior energy storage capabilities (Wang and Xie 2022) compared to sensible heat storage, their manufacturing costs and maintenance expenses pose prohibitive barriers. Sensible heat storage materials have the disadvantage of having little energy density but requiring a large volume (Shringi et al., 2014). However, using sensible heat as an environmentally-friendly and low-cost heat storage provides an advantage of this technology. Sensible heat energy storage is commonly applied for needs with a temperature range of 40-75 °C. Some examples of materials that can be used as standard sensible heat energy storage such as gravel mixed iron scraps (Bhardwaj et al., 2019), sand river and agriculture wastes (Vengadesan and Senthil 2020), pebble stone (Andharia et al., 2022; Chaouch et al., 2018; Raja et al., 2021), rock (Kareem et al., 2022), gravel (El-Sebaai et al., 2007), limestone (El-Sebaai et al., 2007), aluminum scraps (Murali et al., 2020), and water (Moravej and Abdolkarim 2017; Moravej and Fatemeh 2018).

Glazing plays a critical role in the collector system. It has two roles, namely as a trap and as a heat retainer under solar lighting. The air trapped between two glazes provides an insulating effect called an air insulator (Bennour Mzad 2022). This air insulator effect does not occur in single glazing. Heat loss occurs when the glazing surface has a higher temperature than the ambient temperature (Chen et al., 2021; Subiantoro and Ooi 2013). Double-glazing technology becomes an alternative for reducing the impact of heat loss. In the collector system, double glazing can increase the heat coming out of the collector (Yang et al., 2023). Generally, double glazing is used for constructing window needs (Chen et al., 2021), but switching the application as a collector that has been done. The research by (Ehrmann Reineke-Koch 2012) revealed that double glazing can reduce emissivity under low-emitting (low-e) conditions. Collectors to increase heat loss resistance during solar irradiation are suggested to use

low-e materials with the addition of coatings on the glazing surface (Ehrmann et al., 2013). In addition, double glazing technology can be applied to insulate heat during sunlight and release heat slowly at night, called nocturnal heating (Yang et al., 2023). The application of double glazing conducted by (Yang et al., 2023) can provide efficiency with a range of 34.51–44.49%. As reported by (El-Sebaei et al., 2007), adding double glazing with gravel can only provide 22–27% lesser overall efficiency than similar technologies today. The research conducted by (Krishnananth and Kalidasa 2013) with different configurations showed an increase in efficiency with the duration of irradiation.

To date, within the realm of solar collector development, no studies have explored the integration of air-blowing type flat plate collectors coupled with sensible heat storage material, specifically iron scraps with a density of 250 kg/m<sup>3</sup>, marking a distinctive novelty in this study. The objectives of this research were to (1) determine and compare the temperature characteristics of the glazing, collector room, and iron scraps during passive-active mode irradiation, (2) to determine and compare the energy efficiency of the collector and iron scraps as heat storage material during passive-active mode irradiation, and (3) identify the thermal characteristics and duration of heat release stored in the TES.

## METHOD

### Geographic conditions

This study is highly dependent on the length and strength of solar irradiation. The dependency and unpredictable changes in conditions determined the geographic conditions under which the study was conducted or cancelled. The study was conducted when the morning was cloudless and dark. Predictable irradiation could occur for 7 hours (08.00–15.00 local time). The research was conducted in September 2023 at an average temperature and relative humidity of 30.7% and 38.1 °C. The average wind speed and solar radiation intensity were 1.52 m/s and 982.6 W/m<sup>2</sup>.

### System description

The solar thermal collector was conceptualized with low-cost and passive-active flow methods. The schematic of the heat collector can be

seen in Figure 1. The research was conducted at the Biosystems Mechatronics Laboratory, Faculty of Agricultural Technology, Universitas Brawijaya, Malang Regency (-7.9148106° N, 112.6124469° E). The main components of the heat collector involved double glazing, solar collector, and material energy storage.

### Double glazing

The solar collector cover technology is double glazing type. Double glazing has two parallel glazing to reduce energy loss during irradiation. Its technology could reduce long waves and heat loss. The glazing used is borosilicate glazing with a thickness of 5 mm. The overall glazing dimension was 490×260 mm, and the visible glazing was 480×250 mm. Both panes were placed between frames with a thickness of 5 mm coated with stainless steel with dimensions of 14,98×40 mm (0.7 mm thick stainless steel). The distance between the glazing has a height of 10 mm and was filled with environmental air and pressure.

### Solar collector

The solar collector component comprised double glazing, collector chamber, and absorber. The solar collector room is a space with no other components, and as an accumulation of solar radiation energy that was converted into heat energy, the input air will naturally flow in the collector room and out at the output hole. The solar collector, in its entirety, had dimensions of 502×720×200 mm, with a uniform wall thickness of 32.5 mm. However, the collector chamber exhibits dimensions of 502×205×60 mm. In addition, the heat absorber used is aluminum type with a thickness of 1 mm. The flat plate type absorber was painted in black color all over the surface of the plate. The flat plate has dimensions of 502×205 mm and was mounted on iron material with support for the input and output holes of the collector wall. The heat collector was then installed with an inclination angle of 22°. The tilt angle was determined based on the average perpendicular angle during irradiation at 08:00–15:00 local time.

### Energy storage unit

The iron was selected as the heat storage material. The heat storage chamber is part of the heat

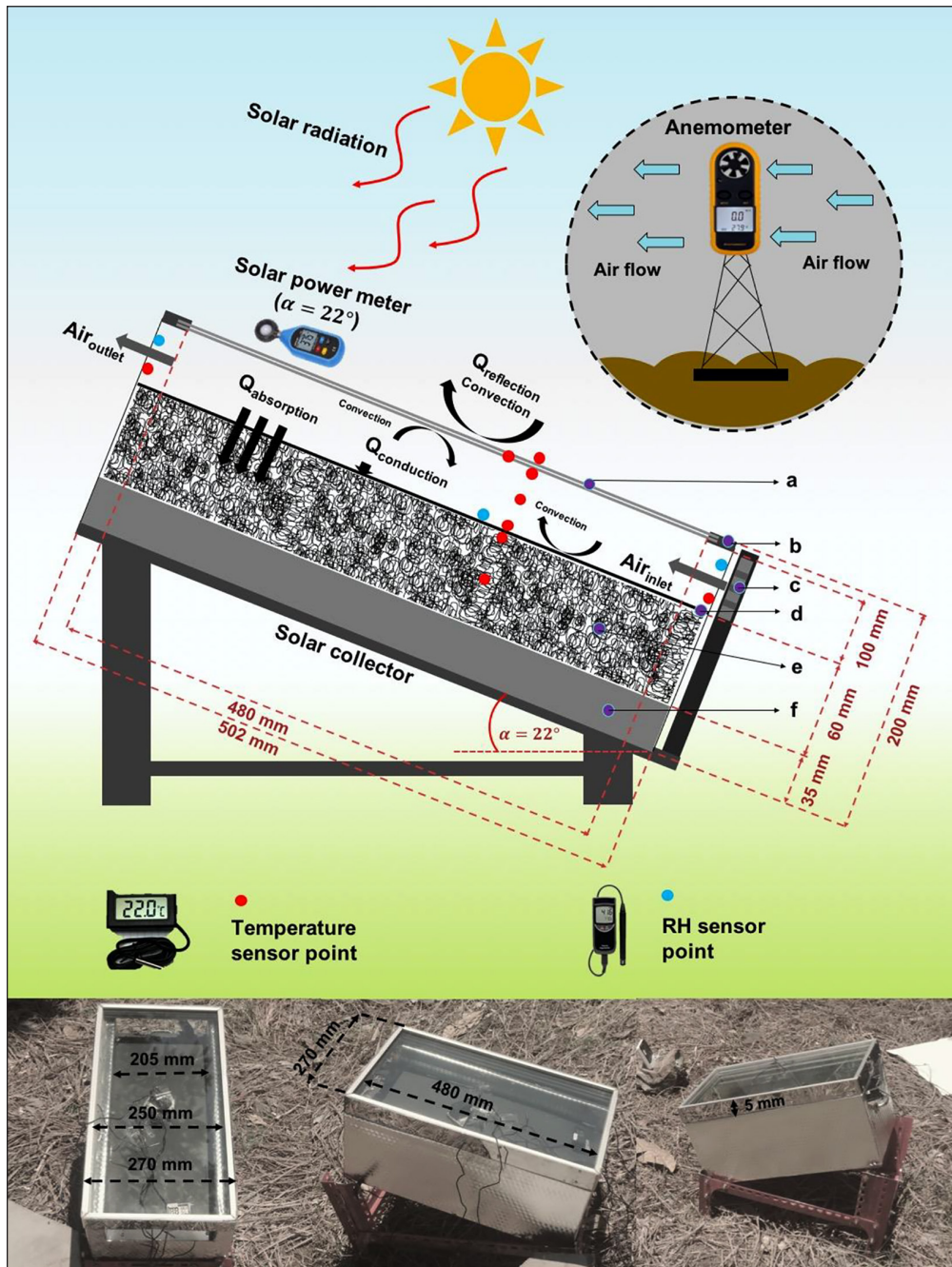


**Figure 1.** Schematic representation of collector with sensor points; (a) glazing cover/ double glazed, (b) frame, (c) external fan, (d) absorber, (e) iron, and (f) insulation

collection collector at the bottom. It has dimensions of 437×205×140 mm. The heat storage material was iron scraps from the motorcycle spare part turning industry in Malang City, Indonesia. Iron scraps were cut into 1–3 cm pieces to facilitate pressing.

### Tool preparation and pressing

The heat collector tool that has been designed and built was then installed with other primary and supporting components. The main

components involved the collector cover (double glazing type), absorber, and heat storage. In particular, the iron scraps were pressed to a pre-determined density of 250 kg/m<sup>3</sup>. Pressing iron scraps was done with a wooden block until solid with dimensions of 437×205×30 mm. Each side of the solid iron scraps with heat storage space has a gap of 2 mm. The heat storage material was pressed, then covered with an aluminum absorber and locked with couplers at the ends of the absorber.

## Sensor installation

The heat collector was installed with 14 sensors consisting of 10 temperature sensors and four relative humidity sensors. The temperature sensors were also installed on the glazing surface, between the glazing, under the glazing, collector chamber, absorber surface, absorber, heat storage material, input air, output air, and environment. Then, four humidity sensors were installed at the input air outlet, collector space, output air outlet, and environment. The sensors were neatly installed, and the display head of the sensor value reading was arranged. The study also added solar radiation and air velocity measurement sensors.

## Data acquisition procedure

The study was conducted in September 2023 with favorable environmental conditions according to the geographical criteria. The data acquisition procedure was based on the values of the 14 measurement sensors described earlier. Temperature and humidity sensors were installed on each part of the heat collector. Illumination, environmental temperature, and humidity sensors were placed not far from the heat collector, as far as 1 m to the right of the heat collector and 0.5 m from the ground. The aim of placing this instrument was to obtain environmental data around the heat collector. Then, the solar power meter instrument was placed on the glazing surface of the heat collector at a slope 22°. The anemometer instrument was placed on a pole at a height of 2 meters from the ground as far as 1 m from the solar collector. During sunlight, all data measured and displayed on the instrument display were recorded for 7 hours (08:00–15:00 local time) with measurements every hour. The same study was conducted for both passive and active operating modes. Measurement during discharging or heat loss in iron materials (TES) utilized a temperature sensor to identify the duration of use and heat behavior during discharging. The temperature sensor was installed in the middle of the iron scrap material

as the heat center in TES. The heat collector was heated under the sun until the iron scraps reached a temperature of 49.5–51.0 °C and then placed in a location protected from the sun to measure changes in temperature using TES. Temperature changes in TES were measured every five minutes until the temperature drops to 29–30 °C.

## Instrumentation

Table 1 shows the instruments and tool specifications used in the study. A total of 10 calibrated thermocouple temperature sensors used an accuracy of  $\pm 0.1$  °C (type FY-10, China) with a measurement range of 0–99 °C. Four RH sensors used a mini digital hygrometer gauge (type FY-12, China) with an RH accuracy of  $\pm 1\%$  and a 10–99% measurement range. The amount of solar radiation during irradiation using a solar power meter (TM-207, Tenmar, Taiwan) with an accuracy of  $\pm 10$  W/m<sup>2</sup>, where the maximum measurement is up to 2,000 W/m<sup>2</sup>. Then, the wind speed measurement employed a fan speed anemometer (Victor-816, China) with an accuracy of  $\pm 0.1$  m/s, which could measure speeds in the 0–30 m/s range.

## Energy analysis

Drying conditions were assumed to be in a steady flow state.  $Q_{in}$  is the energy entering the collector surface ( $Q_{in}$ , J), written in the following equation.

$$Q_{in} = \tau \alpha I_{sc} A_{sc} \quad (1)$$

where:  $\tau$  is the transmissivity (0.85),  $\alpha$  is the absorptivity of the absorber plate (0.95),  $I_{sc}$  is the intensity of radiation falling on the drying chamber (W/m<sup>2</sup>), and  $A_{sc}$  is the surface area covered by the radiation intensity (m<sup>2</sup>).

Solar collector efficiency is the ratio of energy absorbed by the fluid to solar energy in radiation. It is defined in the following equation (Andharia et al., 2022; Malakar et al., 2021; Tong et al., 2016).

$$Q_{sc} = \dot{m}_a C_p (T_{Co} - T_{Ci}) \quad (2)$$

**Table 1.** Instruments used for measurements and specifications

| Components        | Specification | Range                        | Accuracy                  | Manufacturer |
|-------------------|---------------|------------------------------|---------------------------|--------------|
| Thermocouple      | FY-10         | 0–99 °C                      | $\pm 0.1$ °C              | China        |
| Anemometer        | Victor-816    | 0–30 m/s                     | $\pm 0.1$ m/s             | China        |
| Hygrometer        | FY-12         | 10–99%                       | $\pm 1\%$                 | China        |
| Solar power meter | TM-207        | up to 2,000 W/m <sup>2</sup> | $\pm 10$ W/m <sup>2</sup> | Taiwan       |

$$\dot{m}_a = \rho \dot{V} \quad (3)$$

$$\dot{V} = A_C v \quad (4)$$

$$\eta_{SC} = \frac{Q_{SC}}{A_{SC} I_{SC}} = \frac{\dot{m}_a C_p (T_{Co} - T_{Ci})}{A_{SC} I_{SC}} \quad (5)$$

where:  $Q_{SC}$  is the energy in the collector chamber (J),  $\dot{m}_a$  is the mass flow rate of air (kg/s),  $C_p$  is the specific heat of air (J/(kg·K)),  $T_{Co}$  is the temperature of the airflow leaving the collector chamber (°C),  $T_{Ci}$  is the temperature of the air entering the collector chamber (°C), and  $\eta_{SC}$  is the efficiency of the flat plate collector (%).

The heat storage material could be estimated theoretically. The mass flow rate flew by natural or forced convection along the collector. Thermal energy storage in iron scraps stored energy only in sensible heat. This problem was calculated from iron scraps' density, specific heat, as well as the void ratio between the storage space and the heat storage material. The net energy in iron scraps stored during irradiation can be seen in the following equation (Andharia et al., 2022).

$$Q_{t,SHS} = \int_0^x (\rho C_p)_{iron} (1 - \phi) (T_{iron} - T_{iron,in}) dt = [(\rho C_p)_{iron} (1 - \phi) (T_{iron} - T_{iron,in})] x \quad (6)$$

where:  $x$  is the time (hours) and the void ratio ( $\phi$ ) between the compacted iron scraps and the collector heat storage space was calculated using the following equation.

$$\phi = \frac{V_{TES} - V_{SHS}}{V_{TES}} \quad (7)$$

where:  $\rho$  is density (density, kg/m<sup>3</sup>),  $C_p$  is specific heat (J/(kg·K)),  $\phi$  is void ratio,  $T_{iron}$  is temperature of iron waste as material thermal storage (°C), and  $T_{iron,in}$  is temperature input of iron waste (°C),  $V_{TES}$  is volume of

thermal energy storage (m<sup>3</sup>), and  $V_{SHS}$  is volume of sensible heat storage (m<sup>3</sup>).

The net heat recovery used ( $Q_r$ , J) in the thermal energy storage material depends on the water evaporated from the product when it is not in bright conditions, as described by the following equation.

$$Q_r = \int_0^x (m_w)_n h_{fg} dt \quad (8)$$

where:  $h_{fg}$  is the latent heat of evaporation (J/kg),  $n$  is the condition of no light, and  $m_w$  is moisture evaporates (kg). The heat energy storage material's overall energy efficiency ( $\eta_{TES,\%}$ ) is written in the following equation.

$$\eta_{TES} = \frac{Q_r}{Q_{t,SHS}} \quad (9)$$

## Experimental uncertainty analysis

Several factors, such as the selection of instruments in measuring environmental conditions during measurements, may cause error and uncertainty. In order to provide accuracy in collector experimental measurements, uncertainty analysis is mandatory. The uncertainty in the independent variables can be seen in Table 2. The equation for determining the uncertainty of measurement parameters is written in the following equation.

$$W_R = \left[ \left( \frac{\partial R}{\partial x_1} w_1 \right)^2 + \left( \frac{\partial R}{\partial x_2} w_2 \right)^2 + \left( \frac{\partial R}{\partial x_3} w_3 \right)^2 + \dots + \left( \frac{\partial R}{\partial x_n} w_n \right)^2 \right]^{0.5} \quad (10)$$

where:  $W_R$  is the result of measurement uncertainty,  $w$  is the uncertainty in the independent variable, and  $x$  is a function of the independent variable.

## RESULTS AND DISCUSSION

### Geographic conditions

Geographic conditions are a critical parameter in this study. The general parameters measured are solar irradiation, wind speed, environmental temperature, and relative humidity. They have a significantly close correlation with each other. The research conditions were conducted for six days on 14th–19th September 2023. The research weather on 14<sup>th</sup>–19th September 2023 tended to be cloudy during the day until the afternoon. Generally, from day until evening, it tended to be cloudy, but the intensity of solar irradiation was still high.

**Table 2.** Uncertainty in the independent variable

| Parameters  | Uncertainty |
|---|-------------|
| Uncertainty in temperature measurements (°C)                    | ±1.11       |
| Uncertainty in solar radiation measurements (W/m <sup>2</sup> ) | ±23.29      |
| Uncertainty in relative humidity measurements (%)               | ±3.03       |
| Uncertainty in wind speed measurements (m/s)                    | ±0.19       |
| Uncertainty in heat storage material efficiency (%)             | ±0.47       |
| Uncertainty in solar collector efficiency (%)                   | ±0.12       |

The average environmental characteristics during the research can be seen in Figure 3. At the research site, the average solar irradiation levels during passive and active operating modes were measured at 823.7 W/m<sup>2</sup> and 853.8 W/m<sup>2</sup>, respectively. Correspondingly, the average temperatures experienced during passive and active operation stand at 38.4 °C and 38.2 °C, while the average relative humidity levels were recorded at 34.3% and 33.7%, respectively. Furthermore, the environmental average wind speeds during passive and active operation were 1.2 m/s and 1.4 m/s, respectively.

Figure 2 depicts the correlation of each observation parameter between solar irradiation, environmental temperature, wind speed, and

relative humidity presented in an integrated as well as unified manner. Solar radiation affects environmental temperature and RH. It was directly proportional is directly proportional to environmental temperature and inversely proportional to RH. In the morning, solar radiation was still low, thus the temperature and RH values were also low. During the day, there was an increase in solar irradiation and temperature, coupled with a decrease in relative humidity, followed by a reversal of these trends post-daytime irradiation (Ebrahimi et al., 2021; Hawa et al., 2021; Jahromi et al., 2022; Malakar et al., 2021; Singh et al., 2021; Zhou et al., 2023). However, solar irradiation only influenced wind speed and tended to increase in the afternoon.

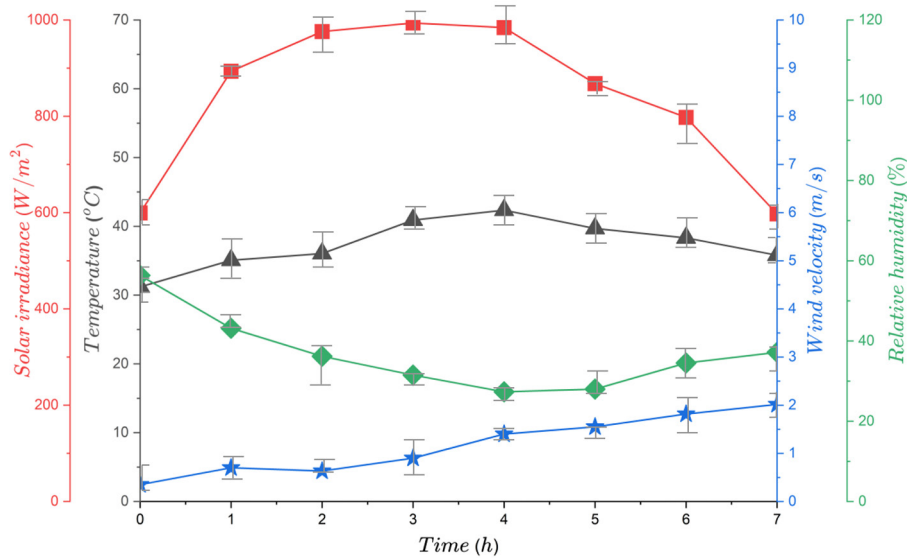


Figure 2. Geographic conditions during the study

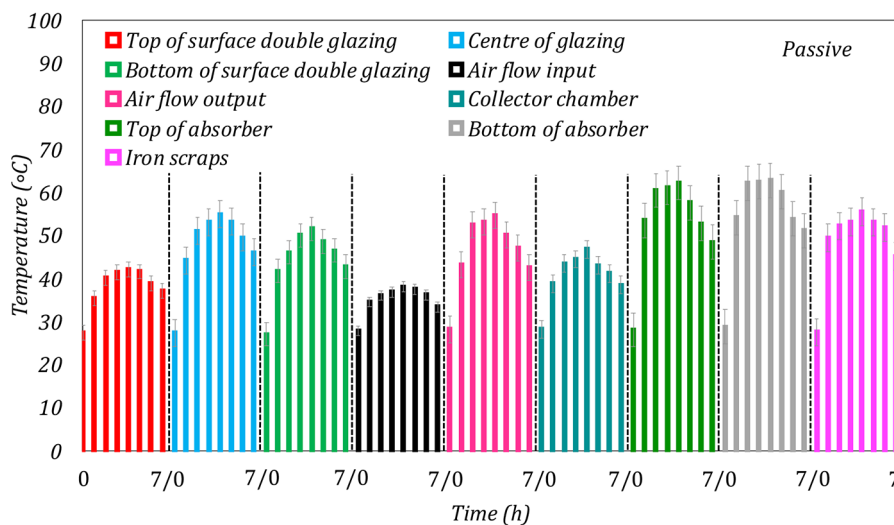


Figure 3. Temperature characteristics of the heat collector during irradiation in passive mode

## Double glazed

The characteristics of double glazing during exposure in passive and active operating modes can be seen in Figures 3 and 4. The average temperature on the surface of the glazing and the space between the glazing and under the glazing in passive mode are 38°C, 47°C, and 44 °C, respectively. The average temperatures on the surface of the glazing, the space between the glazing, and the bottom of the glazing in active mode are 35 °C, 40 °C, and 35 °C, respectively. The results of further analysis show that the penetration rate on the glazing surface is the highest, by 7.9 °C/hour in passive mode and 7.2 °C/hour in active mode in the first hour of sunlight. It provided a penetration rate of 8.89% in passive mode, which was more significant than in active mode. Then, the heat penetration rate in the space between the glazing showed the highest, namely 16.8 °C/hour in passive mode and 13.8 °C/hour in active mode in the first hour of sunlight. In passive mode, the penetration rate was 17.86% greater than in active mode. In addition, the highest penetration rate under glazing was 14.7 °C/hour in passive mode and 11.0 °C/hour in active mode in the first hour of exposure. In passive mode, the penetration rate was 25.17% greater than in active mode. In particular, the temperature behavior of the collector's glazing shows that a low penetration rate indicates a higher heat loss during irradiation, and a high penetration rate indicates low heat loss during solar irradiation.

Double glazing has three parts: the first layer of glazing, the second layer, and a static air cavity between the glazing. This study utilized a collector cover model with double-glazing technology. Double glazing provides a space filled with static air that does not move quickly, which provides a weak insulating effect to reduce heat loss during the measurement process (Bennour and Mzad 2022). This insulator effect became the main reason for selecting this technology. The surface temperature of the glazing is lower than the temperature of the bottom of the glazing. However, the static air cavity temperature is higher than the glazing temperature. The surface temperature of the glazing is lower due to the convection of environmental air passing through it.

Meanwhile, the temperature of the lower glazing closely approximates that of the hollow chamber due to the limited contact between the heat traversing through the glazing and the convection air within the collector chamber.

However, the temperature between the glazing was very high due to the accumulation of input energy when solar radiation waves enter the collector space. The measured thermal characteristics data informs that the surface temperature of the glazing was lower than under glazing, which indicates that heat loss may be slight (Chen et al., 2021; Subiantoro and Ooi 2013).

## Collector's room

The collector space consists of inlet air holes, output air holes, collector space, absorber surface, and bottom of the absorber. The temperature characteristics of each part of the collector chamber can be seen in Figures 3 (passive) and 4 (active). The average temperatures of the inlet air hole, output air hole, collector chamber, absorber surface, and bottom of the absorber in passive mode are 35 °C, 46 °C, 41 °C, 53 °C, and 54 °C, respectively. The average temperatures of the inlet air hole, output air hole, collector chamber, absorber surface, and bottom of the absorber in active mode are 34 °C, 42 °C, 37 °C, 47 °C, and 48 °C, respectively.

The rate of heat penetration from environmental air entering the collector due to the influence of environmental temperature shows the highest temperature of 6.7 °C/hour in passive mode and 5.7 °C/hour in active mode. As a result of heating the air passing through the collector, the input air increased with the highest penetration rate of 15.1 °C/hour in passive mode and 11.8 °C/hour in active mode. Passive mode provides 21.85% higher influence compared to active mode. The heat from solar radiation captured in the upper absorber shows a 25.4 °C/hour penetration rate in passive mode and 17.7 °C/hour in active mode. The accumulated heat provides an average increase of 10.6 °C/hour in the passive model and 6.8 °C/hour in the passive mode. Passive mode provides 35.85% higher influence compared to active mode. A critical collector component in receiving heat waves is the absorber part, where the surface flat plate absorber has the highest penetration rate of 25.4 °C/hour in passive mode and 17.7 °C/hour in active mode. Passive mode provides 30.32% higher influence compared to active mode. Unlike the surface absorber, the bottom absorber has thermal characteristics with different values. The thickness of the plate influences this condition. The highest penetration rate was 25.4 °C/hour in passive mode and 18.7 °C/hour in active mode. Passive mode provides a difference effect of 26.38%

compared to active mode. The penetration rate on the two absorber surfaces differs because the active mode has faster heat loss, disrupting the heat accumulation process.

The studies that have been carried out (Vijayan et al., 2020) show that variations in mass flow rate of 0.01–0.08 kg/s produced temperature differences that come out after passing through the absorber. They revealed that a high mass flow rate caused a low output temperature gain. In addition, the output temperature characteristics following solar irradiation energy were also reported in their study. Natural convection during the heating process in the collector also affects the temperature gain produced by a collector, which is never stable at any time. The temperature characteristics that occur during irradiation on the collector follow the characteristics of solar irradiation at the time of measurement (Channa and Shashi 2022).

### Heat storage material

The characteristics of heat storage materials in the form of iron scraps in passive and active modes can be seen in Figures 4 and 5. The average temperature of iron scraps during irradiation in passive and active modes is 49 °C and 42 °C, respectively. The results of further analysis of the heat penetration rate show that the heat storage material in the passive mode is higher than in the passive mode in the first two. The highest heat penetration rate in passive mode occurs in the first hour of exposure, 22 °C/hour. Then, the highest heat penetration rate in the active model was in the second hour of by 19 °C/hour. The difference between the two modes is up to 13.64% compared to the passive mode. However, the heat penetration speed in both modes has the same value, 5 °C/hour. This condition indicates

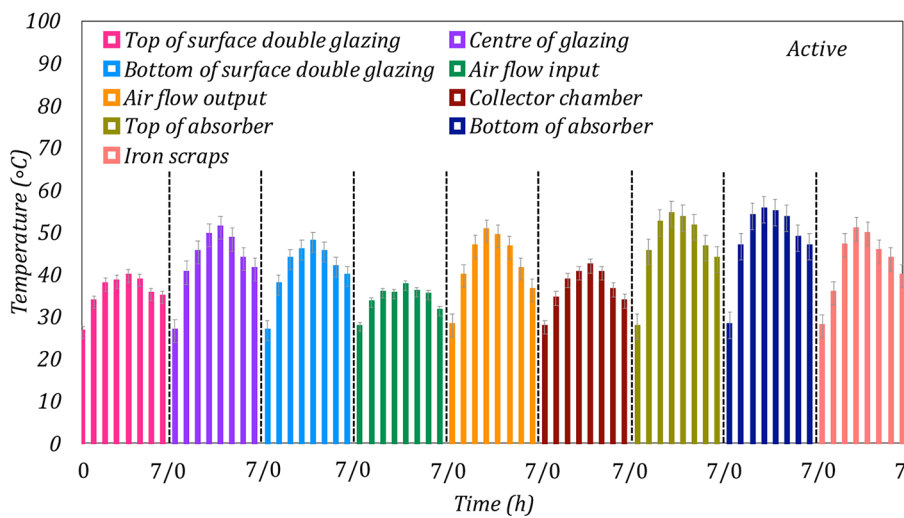


Figure 4. Temperature characteristics of the heat collector during irradiation in active mode

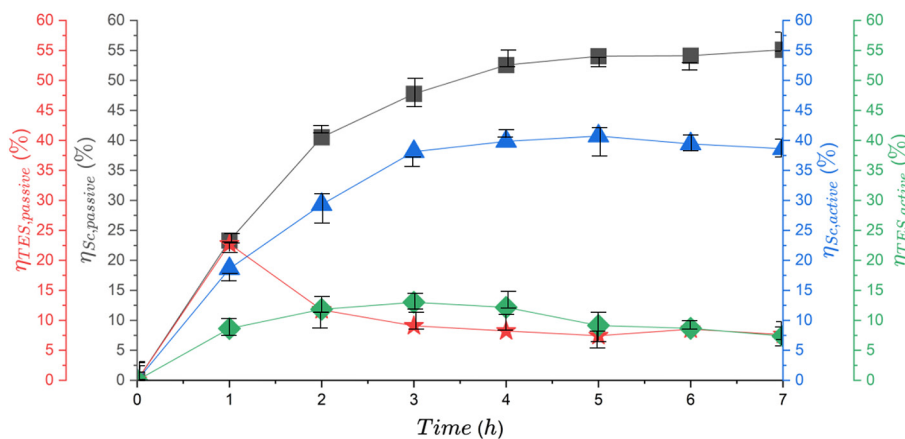


Figure 5. Energy efficiency at the collector and TES during irradiation

that heat penetration into the heat storage material during irradiation has an equilibrium that is not significantly different but only has a significantly different equilibrium time.

Passive mode tends to have a higher temperature compared to active mode. The temperature characteristics of iron scraps relative to the exposure time show that they increase until noon and decrease until they end. This phenomenon follows the behavior of the Sun during morning to evening light (Bhardwaj et al., 2019; Channa and Shashi 2022; El-Sebaï et al., 2007). However, this phenomenon explains that there is an indication that in the afternoon there is a significant heat loss indication in the iron scraps.

### Energy efficiency

The investigation results show that the average energy penetrating the collector is 28.58 kJ (passive) and 28.84 kJ (active). However, the energy utilized in passive and active modes is 14.16 kJ (49.53%) and 10.66 kJ (36.97%), respectively. Figure 5 represents the energy efficiency of the collector and TES during irradiation in active and passive operating modes. The collector has an average efficiency in passive and active mode, 40.93% and 30.58%, respectively, with the highest efficiency being 55.12% and 40.73%. In addition, TES has an average efficiency in passive and active mode of 9.43% and 8.85%, respectively, with the highest efficiency being 22.74% and 13.01%.

The energy efficiency of a collector integrated with sensible heat storage material can be related to the amount of heat storage material used. The results of the research conducted (Chaouch et al., 2018) show that the mass of the heat storage material influences the average daily efficiency. They revealed that using additional and more pebble stones can reduce efficiency and, under certain mass conditions, results in high heat storage efficiency. Iron scraps were less efficient than pebble stone, around 20–71% (Channa and Shashi 2022; Chaouch et al., 2018). However, the results of the research conducted by (Bhardwaj et al., 2019) using iron scraps had an efficiency of 9.8%. This result is similar to this study by 9.4%. They also revealed that the efficiency characteristics during irradiation on flat plate collectors follow the characteristics of solar irradiation from morning to evening. Furthermore, the conductivity value of iron is tremendous, thus the heat transfer that occurs is comparable, which caused the efficiency of iron scrap to be smaller.

### The effect of density on discharging

Variations in the density of iron scrap as TES have different characteristics. Figure 6 illustrates the characteristics of heat release in iron scrap media with various density variations. The release of heat results in a decrease in temperature to 29–30°C. In active operating mode, the iron density of 250 kg/m<sup>3</sup> and 300 kg/m<sup>3</sup> has a slower decrease than the iron density of 200 kg/m<sup>3</sup>. The

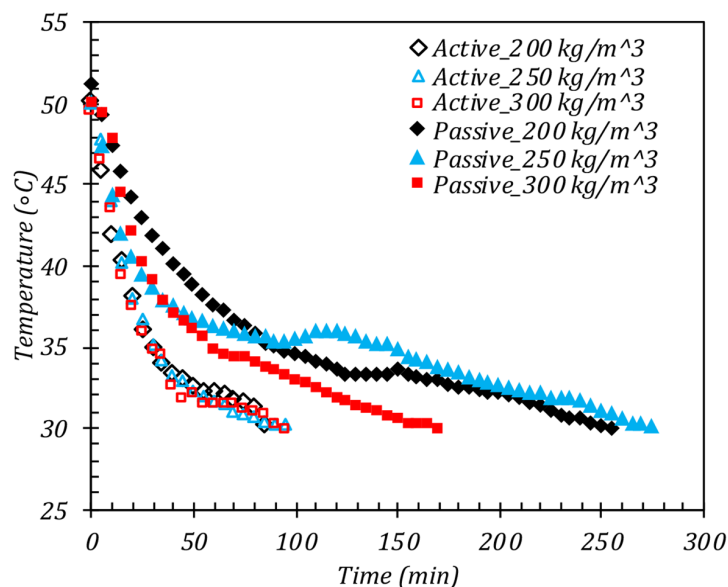


**Figure 6.** Discharging characteristics of iron media as a heat storage material with variations in iron density

heat loss time to the limit of 29–30°C shows that the iron density is 250 kg/m<sup>3</sup> and 300 kg/m<sup>3</sup> for 95 minutes. This condition is longer compared to the iron density of 200 kg/m<sup>3</sup> for 85 minutes. In passive operating mode, iron densities of 200 kg/m<sup>3</sup>, 250 kg/m<sup>3</sup>, and 300 kg/m<sup>3</sup> can release heat for 255 minutes, 275 minutes, and 170 minutes respectively. There are optimum conditions for heat release at an iron density of 250 kg/m<sup>3</sup>. However, the comparison of the operating modes shows that the passive mode can slow down heat transfer, which results in the heat being stored in the iron scrap being longer.

The speed of heat release was influenced by the type of material, density, surface area, particle size, transfer coefficient, and conductivity (Gomaa et al., 2023). At high density, the surface area of iron scraps increases, followed by an increase in thermal conductivity. Under such conditions, the heat stored in the iron scraps will increase the heat transfer released to the absorber surface, which will be used to heat the air passing through it. In passive mode, heat transfer occurred more slowly compared to active mode. In passive mode, measurements were not carried out with a fan, which indicates air passing through the absorber naturally at a low flow rate. Meanwhile, in active mode, air was forced to pass through the absorber surface at high volume and speed, which increased heat transfer speed.

## CONCLUSIONS

A novel collector has been successfully created and investigated in this study. The passive operating mode has higher temperature characteristics than the active mode. All collector sections investigated reveal that the highest temperature found in the absorber. Passive operating mode has better energy efficiency at the collector and TES than active mode. In passive mode, the energy utilized is 49.53%, with an average efficiency of 40.93% (collector) and 9.43% (TES). The results of discharging analysis on iron scraps show that passive mode with a density of 250 kg/m<sup>3</sup> can extend the heat transfer time. In the development of solar collectors temperature became one of the difficult factors to control. Many researchers have carried out collector models and designs to store heat as long as possible for use at night. However, the difficulty in storing heat, especially in sensible heat storage materials such as iron scrap,

poses the greatest challenge in the future. The potential of iron scraps as a heat storage material is excellent to be developed to reduce the iron scraps harmful to the environment as part of an environmentally friendly and low-cost solar collector. In this context, reducing the iron scraps that are not utilized and are often thrown away can be used as a sensible heat storage material for collectors. The collector developed is implemented for a solar dryer for agricultural products. In future studies, the work program on this research panel will isolate the heat absorbed by iron scraps during irradiation. This heat insulation will be developed in a natural composite model made from wood sawdust and bamboo, which is expected to insulate heat better.

## Acknowledgement

This study was funded by LPDP (Indonesia Endowment Fund for Education Agency). Thanks to The Ministry of Finance and LPDP for the support of a doctoral scholarship.

## REFERENCES

1. Ammar, M., Mokni, A., Mhiri, H., Bournot, P. 2022. Parametric investigation on the performance of natural convection flat plate solar air collector with additional transparent insulation material parallel slats (TIM-PS). *Solar Energy*, 231, 379–401. <https://doi.org/10.1016/j.solener.2021.11.053>
2. Andharia, J.K., Markam, B., Dzhonova, D., Maiti, S. 2022. A comparative performance analysis of sensible and latent heat based storage in a small-scale solar thermal dryer. *Journal of Energy Storage*, 45. <https://doi.org/10.1016/j.est.2021.103764>
3. Bennour, F., Mzad, H. 2022. A numerical study of the double-glazed solar air heater (DG-SAH) performance using optimized gas-filled interspaces. *Case Studies in Thermal Engineering*, 40, 102492. <https://doi.org/10.1016/j.csite.2022.102492>
4. Bhardwaj, A. K., Kumar, R., Chauhan, R. 2019. Experimental investigation of the performance of a novel solar dryer for drying medicinal plants in Western Himalayan region. *Solar Energy*, 177, 395–407. <https://doi.org/10.1016/j.solener.2018.11.007>
5. Borzuei, D., Seyed, F. M., Abolfazl A., Rouhollah A., Kouros Bagherzadeh. 2021. An experimental and analytical study of influential parameters of parabolic trough solar collector. *Journal of Renewable Energy and Environment*, 8(4), 52–66. <https://doi.org/10.30501/jree.2021.261647.1172>

6. Channa Keshava Naik, N., Shashi Shekar, K.S. 2022. Evaluation and comparison of performance of a solar pebble absorber collector with a conventional flat plate collector. *Materials Today: Proceedings*, 52, 266–273. <https://doi.org/10.1016/j.matpr.2021.08.025>
7. Chaouch, W.B., Khellaf, A., Mediani, A., Slimani, M.E.A., Loumani, A., Hamid, A. 2018. Experimental investigation of an active direct and indirect solar dryer with sensible heat storage for camel meat drying in Saharan environment. *Solar Energy*, 174, 328–341. <https://doi.org/10.1016/j.solener.2018.09.037>
8. Chen, C.Q., Diao, Y.H., Zhao, Y.H., Wang, Z.Y., Zhu, T. T., Wang, T.Y., Liang, L. 2021. Numerical evaluation of the thermal performance of different types of double glazing flat-plate solar air collectors. *Energy*, 233, 121087. <https://doi.org/10.1016/j.energy.2021.121087>
9. Ebrahimi, H., Samimi Akhijahani, H., Salami, P. 2021. Improving the thermal efficiency of a solar dryer using phase change materials at different position in the collector. *Solar Energy*, 220, 535–551. <https://doi.org/10.1016/j.solener.2021.03.054>
10. Ehrmann, N., Reineke-Koch, R. 2012. Selectively coated high efficiency glazing for solar-thermal flat-plate collectors. *Thin Solid Films*, 520(12), 4214–4218. <https://doi.org/10.1016/j.tsf.2011.04.094>
11. Ehrmann, N., Reineke-Koch, R., Föste, S., Giovannetti, F. 2013. The influence of process parameters and coating properties of double glazing coated with transparent conducting oxides on the efficiency of solar-thermal flat-plate collectors. *Thin Solid Films*, 532, 132–140. <https://doi.org/10.1016/j.tsf.2012.11.145>
12. El-Sebaei, A.A., Aboul-Enein, S., Ramadan, M.R.I., El-Bialy, E. 2007. Year round performance of double pass solar air heater with packed bed. *Energy Conversion and Management*, 48(3), 990–1003. <https://doi.org/10.1016/j.enconman.2006.08.010>
13. Fterich, M., Chouikhi, H., Bentaher, H., Maalej, A. 2018. Experimental parametric study of a mixed-mode forced convection solar dryer equipped with a PV/T air collector. *Solar Energy*, 171, 751–760. <https://doi.org/10.1016/j.solener.2018.06.051>
14. Gomaa, M.R., M.R., Njoud, H.A., Mohammed A.A. 2023. Thermal Performance and Efficiency Enhancement in Evacuated Tube Solar Collectors Using Various Nanofluids. *Journal of Renewable Energy and Environment (JREE)*, 10(4), 146–155. <https://doi.org/10.30501/jree.2023.374760.1507>
15. Hawa, L.C., Ubaidillah, U., Mardiyani, S.A., Laily, A.N., Yosika, N.I.W., Afifah, F.N. 2021. Drying kinetics of cabya (*Piper retrofractum Vahl*) fruit as affected by hot water blanching under indirect forced convection solar dryer. *Solar Energy*, 214, 588–598. <https://doi.org/10.1016/j.solener.2020.12.004>
16. Jahromi, M.S.B., Iranmanesh, M., Akhijahani, H.S. 2022. Thermo-economic analysis of solar drying of Jerusalem artichoke (*Helianthus tuberosus L.*) integrated with evacuated tube solar collector and phase change material. *Journal of Energy Storage*, 52, 104688. <https://doi.org/10.1016/j.est.2022.104688>
17. Kareem, M.W., Habib, K., Pasha, A.A., Irshad, K., Afolabi, L.O., Saha, B.B. 2022. Experimental study of multi-pass solar air thermal collector system assisted with sensible energy-storing matrix. *Energy*, 245, 123153. <https://doi.org/10.1016/j.energy.2022.123153>
18. Krishnananth, S.S., Kalidasa Murugavel, K. 2013. Experimental study on double pass solar air heater with thermal energy storage. *Journal of King Saud University-Engineering Sciences*, 25(2), 135–140. <https://doi.org/10.1016/j.jksues.2012.05.004>
19. Mahapatra, A., Tripathy, P.P. 2019. Experimental investigation and numerical modeling of heat transfer during solar drying of carrot slices. *Heat and Mass Transfer/Waerme- Und Stoffuebertragung*, 55(5), 1287–1300. <https://doi.org/10.1007/s00231-018-2492-2>
20. Malakar, S., Arora, V.K., Nema, P.K. 2021. Design and performance evaluation of an evacuated tube solar dryer for drying garlic clove. *Renewable Energy*, 168, 568–580. <https://doi.org/10.1016/j.renene.2020.12.068>
21. Marc, O., Praene, J.P., Bastide, A., Lucas, F. 2011. Modeling and experimental validation of the solar loop for absorption solar cooling system using double-glazed collectors. *Applied Thermal Engineering*, 31(2–3), 268–277. <https://doi.org/10.1016/j.applthermaleng.2010.09.006>
22. Mardiyani, S.A., Sumarlan, S.H., Argo, B.D., Leksono, A.S. 2019. Design of eco-friendly fixed bed dryer based on a combination of solar collector and photovoltaic module. *Nature Environment and Pollution Technology*, 18(1), 21–30
23. Mokhlif, N.D., Eleiwi, M.A., Yassen, T.A. 2021. Experimental investigation of a double glazing integrated solar water heater with corrugated absorber surface. *Materials Today: Proceedings*, 42, 2742–2748. <https://doi.org/10.1016/j.matpr.2020.12.714>
24. Moravej, M., Abdolkarim, S. 2017. An experimental investigation of the efficiency of a stationary helical solar water heater. *Current World Environment*, 12(2), 250–257. <http://dx.doi.org/10.12944/CWE.12.2.08>
25. Moravej, M., Fatemeh, N. 2018. Experimental Investigation of the Efficiency of a Semi-Spherical Solar Piping Collector. *Journal of Renewable Energy and Environment (JREE)*, 5(2), 22–30. <https://doi.org/10.30501/jree.2018.88602>
26. Murali, G., Rama Krishna Reddy, K., Trinath Sai Kumar, M., SaiManikanta, J., Nitish Kumar Reddy,

- V. 2020. Performance of solar aluminium can air heater using sensible heat storage. *Materials Today: Proceedings*, 21, 169–174. <https://doi.org/10.1016/j.matpr.2019.04.213>
27. Panwar, N.L. 2014. Experimental investigation on energy and exergy analysis of coriander (*Coriandrum sativum L.*) leaves drying in natural convection solar dryer. *Applied Solar Energy*, 50(3), 133–137. <https://doi.org/10.3103/S0003701X14030116>
28. Prakash, R., Kamatchi, R. 2023. Design, fabrication and investigations of natural convection step serrated fin plate integrated trough array low-cost collector for solar air heating: An application to agricultural crop drying. *Solar Energy*, 254, 42–53. <https://doi.org/10.1016/j.solener.2023.02.061>
29. Raja Sekhar, Y., Pandey, A.K., Mahbubul, I.M., Ram Sai Avinash, G., Venkat, V., Pochont, N.R. 2021. Experimental study on drying kinetics for Zingiber Officinale using solar tunnel dryer with thermal energy storage. *Solar Energy*, 229, 174–186. <https://doi.org/10.1016/j.solener.2021.08.011>
30. Shringi, V., Kothari, S., Panwar, N.L. 2014. Experimental investigation of drying of garlic clove in solar dryer using phase change material as energy storage. *Journal of Thermal Analysis and Calorimetry*, 118(1), 533–539. <https://doi.org/10.1007/s10973-014-3991-0>
31. Singh, S., Gill, R.S., Hans, V.S., Singh, M. 2021. A novel active-mode indirect solar dryer for agricultural products: Experimental evaluation and economic feasibility. *Energy*, 222, 119956. <https://doi.org/10.1016/j.energy.2021.119956>
32. Subiantoro, A., Ooi, K.T. 2013. Analytical models for the computation and optimization of single and double glazing flat plate solar collectors with normal and small air gap spacing. *Applied Energy*, 104, 392–399. <https://doi.org/10.1016/j.apenergy.2012.11.009>
33. Tong, Y., Kim, H.M., Cho, H.H. 2016. Theoretical investigation of the thermal performance of evacuated heat pipe solar collector with optimum tilt angle under various operating conditions. *Journal of Mechanical Science and Technology*, 30(2), 903–913. <https://doi.org/10.1007/s12206-016-0144-3>
34. Vengadesan, E., Senthil, R. 2020. A review on recent developments in thermal performance enhancement methods of flat plate solar air collector. *Renewable and Sustainable Energy Reviews*, 134, 110315. <https://doi.org/10.1016/j.rser.2020.110315>
35. Vijayan, S., Arjunan, T.V., Kumar, A., Matheswaran, M.M. 2020. Experimental and thermal performance investigations on sensible storage based solar air heater. *Journal of Energy Storage*, 31, 101620. <https://doi.org/10.1016/j.est.2020.101620>
36. Wang, H., Xie, S. 2022. The effect of annular phase-change material layer on the thermal behavior of solar collector tube. *Journal of Energy Storage*, 52, 104948. <https://doi.org/10.1016/j.est.2022.104948>
37. Yang, L., Zhang, N., Yuan, Y., Cao, X., Qian, B., Zeng, C. 2023. A new operating model for improving thermal efficiency of double-glazed solar air-phase change material collector: An experimental study. *Journal of Energy Storage*, 58, 106448. <https://doi.org/10.1016/j.est.2022.106448>
38. Yang, L., Zhang, N., Yuan, Y., Haghghat, F., Dardir, M., Panchabikesan, K., Sun, Q. 2023. A double-glazed solar air-phase change material collector for nocturnal heating: Model development and sensitivity analysis. *Energy and Buildings*, 289, 113070. <https://doi.org/10.1016/j.enbuild.2023.113070>
39. Zhou, H., Cai, J., Zhang, T., Xu, L., Li, Q., Ren, H., Shi, Z., Zhou, F. 2023. Performance analysis on the concentrated photovoltaic /thermal air collector with phase change material and vacuum double-glazing for temperature regulation. *Renewable Energy*, 207, 27–39. <https://doi.org/10.1016/j.renene.2023.03.012>